Structure *14*, 265–274, February 2006 DOI 10.1016/j.str.2005.10.007

The Backrub Motion: How Protein Backbone Shrugs When a Sidechain Dances

Ian W. Davis,[1] W. Bryan Arendall III,[1] David C. Richardson,[1] and Jane S. Richardson[1,*]
[1] Department of Biochemistry
Duke University
Durham, North Carolina 27710

Summary

Surprisingly, the frozen structures from ultra-high-resolution protein crystallography reveal a prevalent, but subtle, mode of local backbone motion coupled to much larger, two-state changes of sidechain conformation. This "backrub" motion provides an influential and common type of local plasticity in protein backbone. Concerted reorientation of two adjacent peptides swings the central sidechain perpendicular to the chain direction, changing accessible sidechain conformations while leaving flanking structure undisturbed. Alternate conformations in sub-1 Å crystal structures show backrub motions for two-thirds of the significant Cβ shifts and 3% of the total residues in these proteins (126/3882), accompanied by two-state changes in sidechain rotamer. The Backrub modeling tool is effective in crystallographic rebuilding. For homology modeling or protein redesign, backrubs can provide realistic, small perturbations to rigid backbones. For large sidechain changes in protein dynamics or for single mutations, backrubs allow backbone accommodation while maintaining H bonds and ideal geometry.

Introduction

A large body of experimental dynamics data, especially nuclear magnetic resonance (NMR) measurements (Cavanagh et al., 1996; Wuthrich, 1986), shows that a protein molecule in solution is quite mobile, at a range of sizes and timescales. A major driving force for residue-scale mobility is the constant bombardment by solvent and other molecules, felt especially by surface sidechains that dance between favorable conformations (rotamers) under that bombardment and transfer some of those forces to their local backbone. Indeed, sidechains are seen to be more highly mobile than backbone by NMR (Kay, 2005; Palmer, 2004), and surface sidechain mobility is also evident in crystallographic electron density maps even when it is not explicitly modeled. Analogous structural changes occur over the much longer evolutionary timescale, during which the primary event is a sequence mutation (i.e., sidechain substitution), but the effects propagate to cause shifts in backbone conformation. The combination of exquisite packing (Word et al., 1999a) and relaxed conformations (Lovell et al., 2000, 2003) in protein cores, along with the degeneracy of permissible sequences (Gassner et al., 1996; Lim and Sauer, 1989; Munson et al., 1994), implies that the backbone must exhibit low-energy, localized modes of change that coadapt sidechain and backbone conformations to the new local structural requirements of sequence changes.

In either the dynamic or evolutionary case, however, even something as "simple" as backbone accommodation to local sequence or rotamer change is surprisingly difficult to model accurately. For large-scale backbone motions, various methods can produce approximate results close enough to be of practical utility: molecular dynamics (Karplus and McCammon, 2002; Lipari et al., 1982), elastic networks (Bahar et al., 1997), inverse kinematics (van den Bedem et al., 2005), iterative simulation of fragment combinations (Rohl et al., 2004), and systematic secondary-structure deformations (Qian et al., 2004). However, accurate prediction of local backbone changes has been elusive, which is a problem for several fields. Crystal structures of mutant proteins show conclusively that small backbone rearrangements are indeed very common (Baldwin et al., 1993; Matthews, 1995), but energy calculations are still unable to predict those changes accurately. The detailed interpretation of backbone order parameters measured by NMR dynamics is hampered by the lack of reliable alternative models for local backbone motion. The notable successes of protein redesign (Dahiyat and Mayo, 1997; Desjarlais and Handel, 1995; Looger et al., 2003) mostly depend on limitation to a completely rigid backbone scaffold taken from a known natural structure. Similarly, homology modeling (Tramontano and Morea, 2003) generally works best if the core backbone of the template structure is left unchanged, although we know that the backbone will, in fact, accommodate somewhat (Mooers et al., 2003). Modeling of small, local backbone motion is usually done either with molecular dynamics or with a set of predefined geometrical "moves" such as peptide flips or crankshaft ϕ/ψ motions (Fadel et al., 1995). Problems with these approaches include allowing unrealistic backbone motions (Hu et al., 2003), holding fixed the sidechains and surrounding structure, and not explicitly considering correlated motions of adjacent peptides or coupling with changes of sidechain conformation.

Our attention was first drawn to backbone-sidechain coupling when manipulating brass "Kendrew" models, in which a correlated twist of adjacent peptides is effective for swinging Cα-Cβ bonds up perpendicular to a β sheet. Similar shifts of Cβ directionality were invoked to account for altered near-neighbor packing of aromatic residues in our protein design work (Richardson et al., 1992). When the rebuilding of backward-fit sidechains in crystal structures required adjustment of the Cα-Cβ direction (Richardson et al., 2003), we investigated plausible backbone motions and prototype software tools to accomplish those changes ([Noonan et al., 2004] and Experimental Procedures). Figure 1 illustrates the appearance of such local backbone motion and the geometrical parameters that describe it in our Backrub algorithm. These small backbone and Cβ shifts have been important factors in the success of our structure-improvement methods (Arendall et al., 2005). Until now,

*Correspondence: jsr@kinemage.biochem.duke.edu

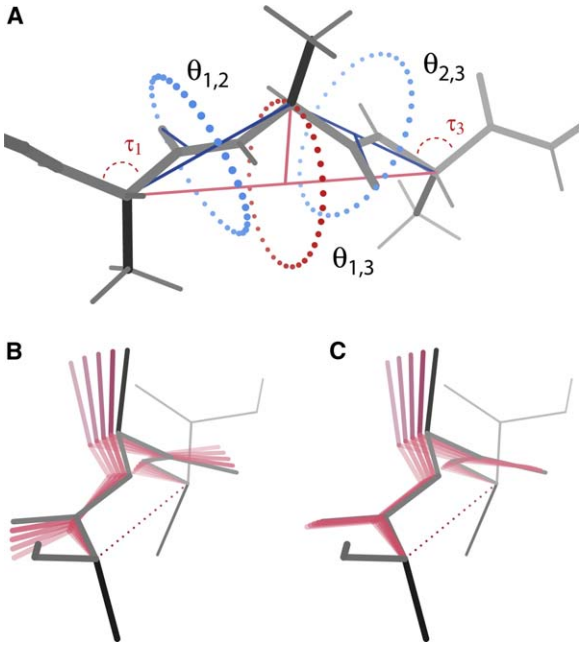

Figure 1. Schematic Representations of the Backrub Motion

(A) A schematic diagram of the Backrub motion. The primary rotation ($\theta_{1,3}$) moves the central residue and its adjacent peptides around the red axis ($C\alpha_{i-1}$ to $C\alpha_{i+1}$) as a rigid body, causing the central $C\alpha$ to trace out the dotted circle. Secondary rotations ($\theta_{1,2}$ and $\theta_{2,3}$) move the individual peptides as rigid bodies around the blue $C\alpha$-$C\alpha$ axes. A small amount of distortion is introduced into the τ angles (N-$C\alpha$-C), but they generally remain well within the range of values seen in typical crystal structures.

(B) A series of backbones generated with Backrub by making 5° steps around the primary rotation axis (hydrogens not shown).

(C) Another series of backbones generated with Backrub by making 5° steps around the primary rotation axis, while also rotating each peptide to roughly maintain the H bonding position of the NH and CO groups.

however, there was no direct evidence as to whether this motion actually occurs in the molecules themselves.

The current study describes the small-scale, local "backrub" motion; shows that the backrub is the most common local backbone change seen in ultra-high-resolution protein structures; describes the Backrub algorithm for modeling such shifts; and shows that this low-energy, small-amplitude concerted shift of the backbone atoms in two successive peptides is coupled to a much larger-scale, two-state change of conformation for the central sidechain. This constitutes one important example of a new paradigm of local backbone motion that is both demonstrably realistic and explicitly sidechain coupled.

Results

A backrub motion shifts the position of the $C\alpha$-$C\beta$ bond vector for residue *i* by a backbone change that is low energy (i.e., maintains essentially ideal bond lengths, bond angles, and peptide planarity) and is purely local (i.e., with essentially no motion of $C\alpha_{i\pm1}$ and none at all beyond $C\alpha_{i\pm2}$). The Backrub modeling algorithm, described in Experimental Procedures, closely satisfies the backrub paradigm using three rotations around $C\alpha$-$C\alpha$ axes, as illustrated in Figure 1.

We first present a survey of backbone plasticity as revealed by the alternate conformations in a set of sub-1 Å resolution crystal structures totaling nearly 4000 residues. These data show that backrub motions are quite common, and that the Backrub algorithm is sufficient to create realistic models that closely match the experimental observations. We then illustrate the process of using Backrub for refitting during the structure determination process. A table of examples (Table S1) is available as Supplemental Data with the online version of this article. Three-dimensional kinemage graphics, selected coordinates, and a Readme file are available as Additional Data at http://kinemage.biochem.duke.edu/suppinfo/StructureDavis2006.

The 19 structures surveyed are described in Table 1. Of the alternate conformations that shift the backbone for a dipeptide or less, 76% are backrub motions (126/166, listed in the Additional Data). Globally, then, 3.2% (126/3882) of all residues in these structures are well modeled as a backrub change in backbone conformation. This is a conservative estimate, omitting examples that can be modeled successfully without $C\beta$ shift (e.g., 1N9B Leu30), but not considering the complementary cases best modeled as significant $C\beta$ shifts but not deposited as such (e.g., 1PQ7 Cys57). Serine is far the most common amino acid seen, making up 25% of backrubs. Two factors could explain their predominance: Ser is the smallest rotatable sidechain, and it has many choices of donor or acceptor H bond partners, some of which are local enough to constrain these slight backbone shifts. Most alternate conformations of any type occur at the protein surface, and polar sidechains predominate; Lys, Arg, and Glu each contribute 8% of backrubs. Of the hydrophobics, Val, Met, and Leu occur most often.

Other types of backbone motions observed include peptide flips (a three peptide change in which the central peptide rotates by 90°–180°), usually in tight turns. They can be identified even within long stretches of concerted motion, but they are still much more rare than backrubs, with only four cases in this data set: 1GWE 105, 1IX9 135, 1MUW 174, and 1US0 93. Intermediate rotations of single peptides are identifiable from large displacements of the carbonyl O density: many can be fit well with the Backrub tool (e.g., 1PQ7 Ser132 and 1US0 Arg40) although the sidechain does not always move (e.g., 1N9B Ser41, which preserves two helix N-cap H bonds through waters; coordinates are available in the Additional Data). The single-residue "other" cases include four large movements of chain-terminal residues, which are unconstrained on one side and thus have very different properties.

Figures 2A and 2B compare two different relationships seen for alternate-conformation serines, the most frequent backrub amino acid. These and other examples are available as animated, 3D kinemage graphics in the Additional Data. Figure 2A shows Ser34 in an $\alpha\beta$ loop of the 1N9B TIM barrel, with a large $C\beta$ shift of 1.02 Å. Alternates were defined for all atoms in residue 34, but not the rest of the two peptides. This represents the changes reasonably well but gives highly nonplanar peptides for which there is no direct evidence; a pair of Backrub models fits the density equally well with nearly ideal geometry. Electron density for the carbonyl oxygen is

Table 1. The Set of Protein Structures Surveyed for Alternate Backbone Conformations

PDB Code	Description	Reference	Resolution, Å	Total Residues	Alternate Residues[a]	Single Alternates[b]	ΔCβ > 0.2 Å[c]	Classifiable Alternates[d]	Backrubs[e]
1EJG	Crambin (valence electron density)	(Jelsch et al., 2000)	0.54	48	19	17	7	6	**5**
1UCS	Type III antifreeze protein RD1	(Ko et al., 2003)	0.62	64	6	6	0	0	**0**
1US0	Human aldose reductase, with NADP+ and inhibitor	(Howard et al., 2004)	0.66	314	79	45	18	16	**10**
1R6J	Syntenin PDZ2	(Kang et al., 2004)	0.73	82	21	12	3	2	**2**
3AL1	Designed peptide α1, racemic P1-bar form	(Patterson et al., 1999)	0.75	24	11	11	7	7	**6**
1IUA	*Thermochromatium tepidum* HiPIP	(Liu et al., 2002)	0.80	83	6	6	2	2	**2**
1PQ7	Trypsin at pH 5 in borax	(Schmidt et al., 2003)	0.80	224	15	12	7	7	**5**
1NWZ	Photoactive yellow protein	(Getzoff et al., 2003)	0.82	125	25	12	8	7	**6**
1N55	E65Q mutant of *Leishmania* triosephosphate isomerase	(Kursula and Wierenga, 2003)	0.83	249	33	31	22	18	**9**
1SSX	α-lytic protease at pH 8	(Fuhrmann et al., 2004)	0.83	198	23	23	17	13	**11**
1MC2	K49 phospholipase A2 homolog	(Liu et al., 2003)	0.85	122	10	10	4	3	**3**
1G6X	Bovine pancreatic trypsin inhibitor with mutated loop	(Addlagatta et al., 2001)	0.86	58	12	12	2	2	**2**
1MUW	Xylose isomerase	(Fenn et al., 2004)	0.86	386	79	70	24	16	**12**
1DY5	Deamidated bovine pancreatic ribonuclease	(Esposito et al., 2000)	0.87	246	39	39	23	22	**21**
1GWE	*Micrococcus lysodeikticus* catalase	(Murshudov et al., 2002)	0.88	498	47	40	9	8	**5**
1F9Y	*E. coli* HPPK with MgAMPCPP and 6-hydroxymethylpterin	(Blaszczyk et al., 2003)	0.89	158	21	21	3	3	**2**
1IX9	*E. coli* Mn(III) superoxide dismutase mutant	[f]	0.90	410	41	34	18	15	**11**
1N9B	Extended-spectrum SHV-2 β-lactamase	(Nukaga et al., 2003)	0.90	265	53	51	19	14	**11**
1OEW	Native endothiapepsin	(Erskine et al., 2003)	0.90	328	29	24	7	5	**3**
Total				3882	569	476	200	166	**126**

[a] Residues with one or more atoms in alternate conformations.
[b] Alternate conformations that encompass, at most, one residue plus its peptides.
[c] Single alternates with Cβ positions separated by at least 0.2 Å in the deposited model.
[d] Alternates with verified Cβ shift > 0.2 Å and clear enough electron density to reliably infer the mode of backbone change.
[e] Classifiable alternates that displayed backrub motion instead of some other type of motion.
[f] PDB file 1IX9 has no published journal reference; the depositors are B.F. Anderson, R.A. Edwards, M.M. Whittaker, E.N. Baker, and G.B. Jameson (2002).

highly anisotropic, indicating a single-peptide rotation that reinforces the primary backrub rotation rather than the usual compensation that preserves backbone H bonding (as in Figure 1C). Ser34 alternate conformations are coupled to those of Arg250 (data not shown), making or breaking an H bond to the Ser Oγ. The Ser sidechain moves but does not change rotamer conformation; this is unusual, since 108 out of 126 backrub cases (86%) show distinct sidechain rotamers, as is also true for most single-residue "other" cases. A total of 87 of the backrubs with distinct rotamers have χ1 in distinct local minima, as seen in Figures 2B and 2D. Backbone alternates without a rotamer change usually show distinct H bond states for either sidechain (Figure 2A) or backbone.

Figure 2B shows 1DY5 SerA15, a more typical serine backrub example with distinct rotamers and H bonds; there is a clear 0.46 Å Cβ shift, implying a backbone movement. Alternates were defined in the PDB file for Cβ, but not for any backbone atoms (white), producing bond-angle distortions of up to 9° around Cα and Cβ. Here, also, a pair of Backrub models (orange) fits the

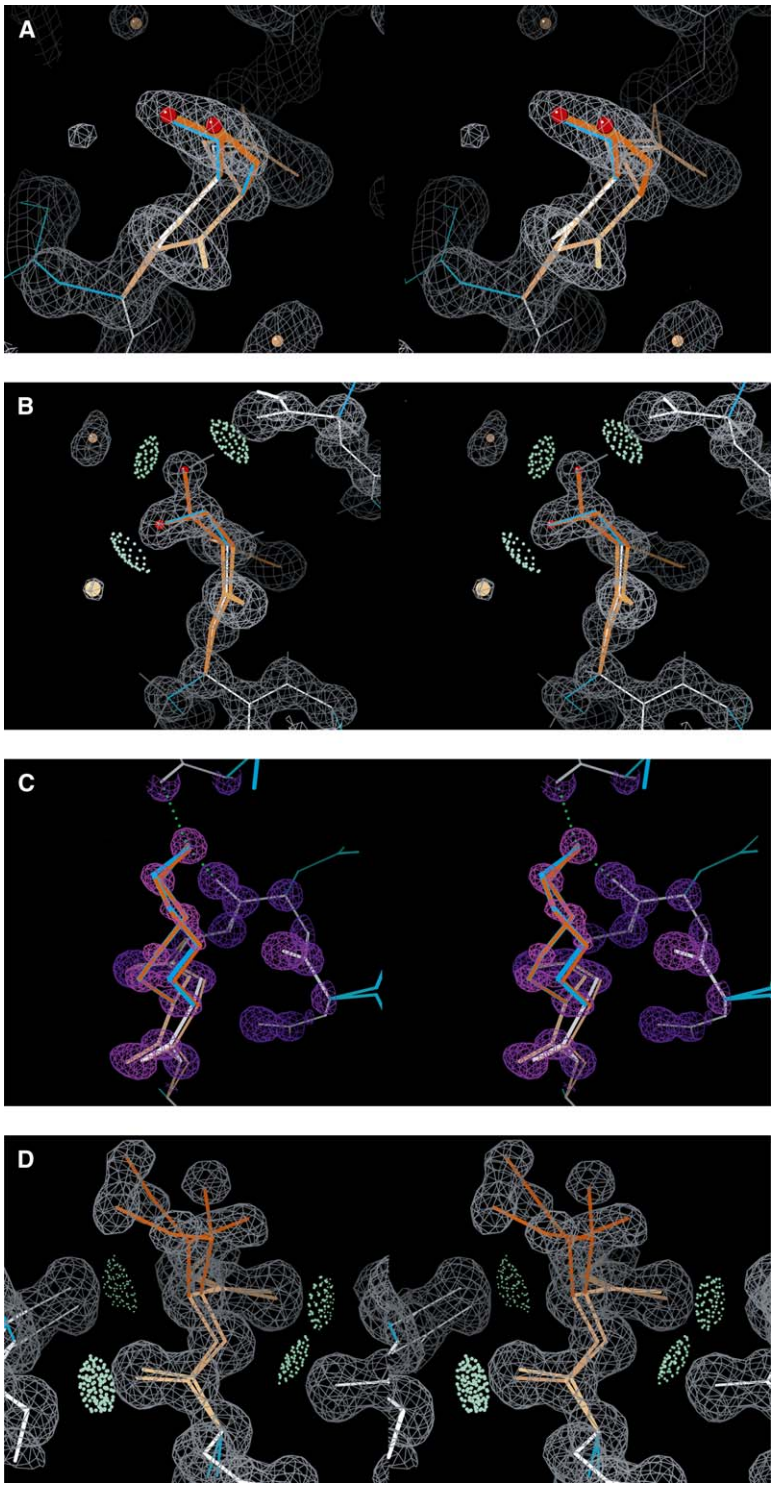

Figure 2. Backrub Motions from Alternate Conformations

(A–D) Examples of backrub motions observed in the alternate conformations of atomic resolution crystal structures for two serines (the most commonly occurring backrub residue), a lysine, and an isoleucine. Original models are in white and cyan; Backrub-fit models are in orange. $2F_o - F_c$ maps contoured at 1.2σ are shown in gray; hydrogens are shown only in (B). See the text for further details. (A) Ser34 from 1N55. This residue moves in concert with Arg250 to make/break an H bond, but it does not change rotamer. (B) SerA15 from 1DY5, which changes both rotamer (χ1 *m* versus *p*) and its H bonding state to nearby backbone and to waters. (C) Lys100 from 1US0, with rotamers *mppt* and *mtmm* both ending at the same H bonded Nζ position. All alternate sidechain atoms show clearly separated density peaks at 3σ (purple contours). (D) Ile47 from 1N9B, in rotamers *tt* and *mm*. Backrub models were fit for both A and B alternate conformations (peach/orange). The deposited model (not shown here) was fit without backbone alternates, but it had a Cβ shift of 0.6 Å and the same two sidechain conformations as shown.

electron density equally well with τ deviations under 1σ (3º) and completely ideal geometry otherwise. The asymmetrical T shape of the sidechain electron density for SerA15 is the usual pattern for serines with Cβ alternates (e.g., 1MUW Ser69, 1DY5 SerB50 in the Additional Data). One conformation (here, with Oγ pointing left) has no strong positive or negative constraints, its rotamer is excellent, and its backbone conformation is presumably relaxed. The second conformation makes a favorable, but constrained, H bond (to a backbone CO) that is not accessible with a good rotamer and good geometry from the other Cβ position. Thus, the second Cβ is pushed back significantly (causing a backrub shift), and the sidechain finds a compromise between H bond strength and a favorable χ1 angle. The Ser15 backbone CO stays in position and H bonded. Ser15 in

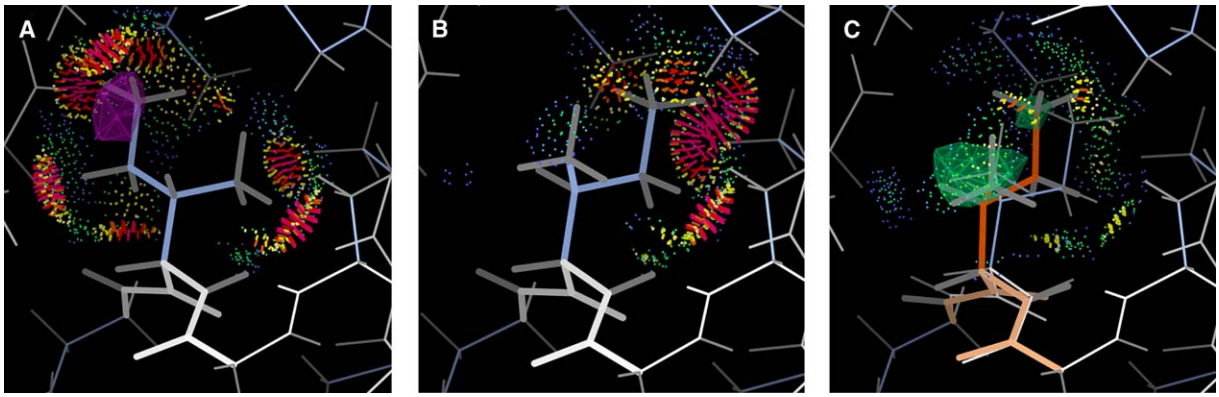

Figure 3. Crystallographic Rebuilding with Backrub in KiNG

(A–C) The Backrub tool in KiNG (Davis et al., 2004) was used to rebuild IleA120 of 1MO0. (A) The original conformation had serious steric clashes (pink spikes) with the surrounding residues and occupied a negative peak in the difference density (magenta). (B) The pt rotamer has clashes on one side and a small cavity on the other. (C) The Backrub model (peach/orange) shifts IleA120 into that empty space and establishes good packing contacts (green and blue dots) with its neighbors; it also satisfies positive peaks in the original difference density (green).

chain B shows the same pattern; that is usually, but not always, the case between subunit pairs with noncrystallographic symmetry.

Lys100 from 1US0 displays even clearer and more extensive alternate-conformation electron density (Figure 2C), with 3σ peaks (purple) for all sidechain atoms in each conformation, including the Cβs that are 0.97 Å apart. Strong anisotropy of backbone density indicates motion of those atoms also. Lys100 combines backbone and sidechain motion to leave Nζ in place (at top in Figure 2C), maintaining two H bonds to backbone carbonyls and a weaker interaction with Asn52 Oδ. The B alternate is a good rotamer (*mtmm*) (Lovell et al., 2000), and the A alternate is an acceptable one (*mppt*). Lys100 forms the C-cap of an α helix (Richardson and Richardson, 1988), and its backbone H bonds are apparently preserved by a concerted, smaller backrub motion of Ser97. Backrub motions are less common and smaller within helices, where steric constraints from neighboring turns limit the magnitude of motion in the backrub direction. They are most common in β strands or extended loops. Another case of concerted backrub motion between two interacting residues is Tyr378 of 1GWE (see the Additional Data), one conformer of which would intersect its 2-fold equivalent in another subunit if both were occupied simultaneously.

Figure 2D shows Ile47 of 1N9B. Well-separated electron density peaks for all six Cγ and Cδ atoms in the two distinct sidechain rotamers unambiguously mandate two Cβ positions and two backbone conformations, which are fit by the two Backrub models (orange/peach) with near-ideal geometry for both backbone and sidechain. This is a prototypical case in which the two peptides counterrotate somewhat against the primary Backrub rotation and preserve all four β sheet H bonds (lenses of green contact dots, with both conformations overlaid in the figure). Another example of sidechain motion with a backrub-maintained β sheet is Thr268 of 1R6J.

In this analysis, several amino acid types are special cases. Glycine was ruled out by definition, since it has no Cβ to show a shift. Only one alanine is represented (1N9B Ala257), presumably because Ala sidechains have neither rotamer nor H bond states to drive local backbone shifts. Cystine alternates are frequently driven by breaking the disulfide; rotamers may or may not change (1PQ7 Cys41 in the Additional Data, 1N9B Cys123). Cys or Met alternates can often be analyzed at somewhat lower resolutions, if the heavy S atoms are clearly visible. Eight prolines have Cβ alternates fit >0.2 Å apart, one alternate in each ring pucker (Cγ endo and Cγ exo). Half of them can be fit well by Backrub, including the skewed relationship of Cγ positions, but it is unclear whether that is the best description. Analysis of proline alternates is hampered by overlapping density for most atoms and by errors (Engh and Huber, 2002) in geometry values currently used for proline (Engh and Huber, 1991), which would cause some bias even at these high resolutions. Arginine displays especially varied and elegant patterns of alternate conformations because of guanidinium size and H bonding (e.g., 1SSX Arg120, 192; 1MUW Arg204).

Figure 3 shows an example of using the Backrub software tool for model rebuilding during crystallographic refinement: IleA120 from 1MO0. In addition to representing real backbone plasticity as shown above, Backrub is also very effective for rebuilding because it moves one Cα and the neighboring peptides by a small amount, but it dramatically alters the accessible rotamers by swinging the entire sidechain on a long lever arm. In the original conformation of Figure 3A, all-atom contacts (Word et al., 1999a, 2000) indicate severe steric clashes with surrounding atoms, and difference peaks in the $F_o - F_c$ map suggest that χ1 is off by 120°. When the correct sidechain rotamer is fit on the original backbone (Figure 3B), the serious steric clashes are all on one side, with space on the other side. A Backrub movement swings the sidechain to establish excellent packing interactions all around (Figure 3C). Additional evidence strongly supports the correction: sidechain rotamericity improves, difference density is satisfied, and the new model matches Ile120 of chain B. Final confirmation comes from improved rerefinement (Arendall et al., 2005).

Discussion

The alternate conformations seen in sub-1 Å resolution crystal structures show unambiguously that protein backbone often exhibits highly localized, small-amplitude plasticity that is tightly coupled to a larger, two-state conformational change of the sidechain. By far the most common case is a "backrub" motion, in which one residue and its adjacent peptides twist slightly around the backbone; this is usually driven by a change in sidechain rotamer and/or hydrogen bonding partners, leading to significant sidechain motion perpendicular to the chain direction. Over the 19 proteins and 3882 residues studied here, 1 residue in 30 clearly shows a backrub motion (126 examples), and backrub motions are surely even more prevalent under physiological or solution conditions than in frozen crystals.

The Backrub algorithm described here produces geometrically and sterically reasonable models that fit the electron density extremely well. Its utility in crystallographic rebuilding is demonstrated in Figure 3 (see above) and in Arendall et al. (2005). In practice, Backrub manipulations are most useful either for defining alternate conformations at very high resolution or for correctional rebuilding of backbone in the 2–3 Å resolution range. At resolutions <2 Å, backbone atom positions are strongly constrained, so a sidechain misfit into the wrong rotamer produces distorted bond angles instead (Lovell et al., 2003). At resolutions >3 Å, one cannot address such fine detail, due to surrounding inaccuracies.

Backrub motion is large for the central sidechain, moderate for its backbone, and decreases rapidly on either side. To accomplish a "true" low-energy backrub movement with essentially pure ϕ,ψ variables, as proteins presumably do, extremely small changes would propagate past the $i\pm1$ Cα atoms. This involves at least five pairs of ϕ,ψ angle changes and an intractable level of complexity. As the figures show, however, Backrub-generated models are remarkably good at fitting the electron density of alternate conformations with only three variables besides sidechain χ angles. Resulting sidechain rotamers (Lovell et al., 2000) are essentially always favorable, and all bond lengths, bond angles, and peptide planarity can be kept ideal, except for the τ bond angles at Cα $i-1$, i, and $i+1$. Those τ distortions seldom exceed one standard deviation (Engh and Huber, 1991), and sometimes ideality is improved. Of course, any Backrub refitting during solution of a crystal structure would be submitted to further refinement afterward. A small percentage of cases appear to require nonideal rotamers or geometry (especially buried Met or disulfides) and may actually have both conformations strained by the tight surroundings rather than both favorable. Different approximate fitting procedures that are commonly used for crystallography include allowing a sidechain to shift independently of the backbone or allowing one residue to shift independently of its neighbors. Those techniques are not significantly simpler than the Backrub, but they produce very large distortions of bond angles or peptide planarity not supported by the data.

It seems likely that other modes of local backbone plasticity remain to be discovered. This is particularly true of α helices, in which backrub motions are less common than in extended structure. Some examples of helix motions combine winding and unwinding to shift a local region sideways without disrupting the overall helix (e.g., 1EJG 6-9), but no other local helix modes were common enough for classification. Peptide flips were observed in loops, but only rarely.

On the evolutionary timescale, local backrub shifts could be an important component of protein robustness to point mutations, accommodating sidechains of different sizes and shapes without radically altering the backbone scaffold. However, it is difficult to observe backrub motions directly by comparing structures of point mutants because the coordinate error between two "identical," but independently refined, structures is a few tenths of an Ångstrom, comparable to the size of the backrub conformational changes (DePristo et al., 2003; Kleywegt, 1999). Thus, we turned instead to the more accurate and quite numerous examples of backrub motion found within single crystal structures. The magnitude of such backbone movement is small: 90% of the examples shift Cβ < 0.8 Å, and 50% of the examples shift by Cβ < 0.4 Å, while Cα and other backbone atoms move half that much or less. However, essentially all cases leverage sidechain atom shifts of 1–8 Å (2.8 Å on average), quite like the change necessitated by a sequence difference. Nearly all local backbone motions in alternate conformations are coupled to sidechain switches between rotamers (86%), which have steric and electrostatic consequences on par with the effects of a point mutation. Thus, we believe that alternate conformations provide a good model of how a backrub motion could be involved in preserving a protein's structure as its sequence evolves. Of even more immediate practical relevance, the backrub motion should provide a conservative backbone "move," of well documented occurrence in accurate experimental structures, to help protein design and homology modeling calculations provide the local backbone adjustments required for successful accommodation of sequence changes.

These observations are also directly relevant to protein dynamics, in spite of their origin in data from highly ordered crystals at cryogenic temperatures. Individual crystal structures are not usually thought of as dynamic, both because crystallization selects only a subset of the conformations populated in solution, and also because, at most accessible resolutions, alternate conformations are manifested only by lowered electron density and are thus seldom modeled in the coordinates. At very high resolution, however, multiple conformations become directly visible (two or occasionally three copies, down to perhaps 10% occupancy in the best cases). At the cryogenic temperatures typical of modern data collection (near 100 K), presumably no large dynamic fluctuations occur in individual molecules, so alternate conformations represent static disorder between molecules, a sample of the conformations present in the room temperature crystal. In the other direction, however, it is quite certain that the conformations seen in these structures are also present in solution; thus, they show the geometry of a valid subset of protein motions.

Crystallographic alternate conformations imply that the states must have comparable energies, since their observable fractional occurrences lie between 1:1 and at most 10:1 (an energy difference of kT yields a 3:1 ratio). For these Cβ shift cases that imply backbone

motion, the mobile sidechain atoms nearly always show clearly separated peaks, implying an energy barrier between the sidechain states. The backbone atoms, in contrast, nearly always show continuous density between positions close in space, implying that the backbone stays within a single local energy well. As shown above, backrub motions also have the important ability to preserve NH and CO orientations that control backbone H bonds, thus preserving secondary structure despite substantial sidechain movement. This set of properties is only shown here to hold for the low-energy subset of motions manifested in high-resolution crystal structures, but it matches well with the properties seen by NMR order parameters and other dynamical measurements: relatively less motion of the highly H bonded peptide NHs than for the carbonyl-Cα bonds (Wang et al., 2003), and greater and more complex motion for the sidechains (Kay, 2005; Palmer, 2004), most of which visit multiple separate rotamer states (Chou et al., 2003). As a detailed description of a common, experimentally verified local movement, backrub fluctuations provide a new model—in addition to out-of-plane amide vibrations (Palmo et al., 2003) or crankshaft peptide motions (Fadel et al., 1995)—for the analysis of NH order parameters, with the valuable feature of built-in coupling to larger sidechain motions.

Spectroscopic methods dominate the experimental study of protein dynamics because they can measure timescales, relative magnitudes, and even energetics of motions. However, any inference about the pattern of movement in space is highly indirect. In contrast, high-resolution crystal structures can give no insight into timescales, but they show a direct image of what atoms are moving where, and they constitute a valuable and largely untapped source of dynamic information. Here, we have used crystallographic alternate conformations to demonstrate a form of local backbone plasticity that appears to dominate small-scale accommodation to sidechain rotamer fluctuations and perhaps also to single-site mutations. These results also strongly imply that backbone and sidechain dynamics should not be analyzed in isolation, since, for at least one common mode, the two are tightly coupled.

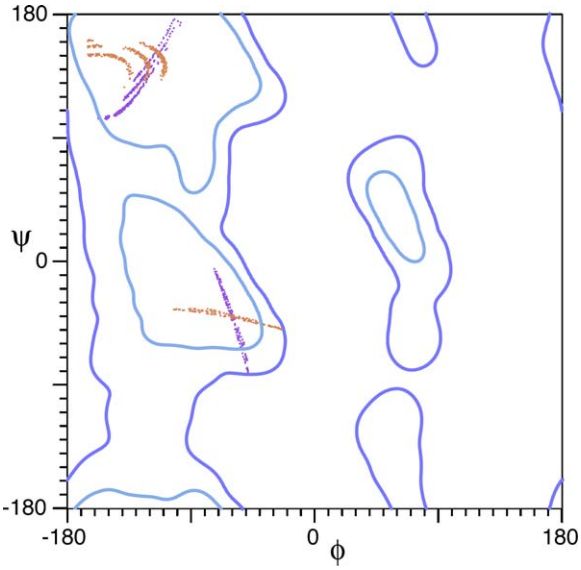

Figure 4. ϕ,ψ Values of Simulated Backrub Motions

ϕ,ψ values for the *i*+1 (orange) and *i*−1 (purple) residues of conformations generated by a brute-force search of ϕ,ψ,τ space with invariant Cα_{i-1} and Cα_{i+1} positions; starting from either an ideal α helix (below center) or an ideal β sheet (top left). The ϕ,ψ angles are plotted within the contours of the updated Ramachandran plot from Lovell et al. (2003); parallel streaks of points result from coarse sampling of τ. All four dihedrals display complex, nonlinear relationships that are highly dependent on the starting conformation.

Experimental Procedures

Survey of Ultra-High-Resolution Crystal Structures

The database consisted of all proteins with deposited structure factors at $\leq$0.9 Å resolution available in the Protein Data Bank (Berman et al., 2000) as of May 2004, excluding duplicates at $\geq$50% identity and short peptides with unusual amino acids. The resulting 19 proteins, containing 3882 residues, are listed by resolution in Table 1. All 19 structure determinations used synchrotron data collected at cryogenic temperatures and refined anisotropic B factors. Phasing methods varied, but all except two were refined with ShelXL (Schneider and Sheldrick, 2002).

Sidechain rotamers are defined and named as for the Penultimate rotamer library (Lovell et al., 2000); "p," "t," and "m" in those names refer to χ angles near +60°, 180°, and −60°, respectively. Structure analysis and creation of display files was done on-line in the MolProbity web service at http://kinemage.biochem.duke.edu/ (Davis et al., 2004; Richardson et al., 2003). If not already present, all hydrogen atoms were added and optimized with Reduce (Word et al., 1999b), but without flips of Asn/Gln/His orientation. All-atom contacts were calculated by Probe (Word et al., 1999a), giving scores and displays for H bonds, van der Waals contacts, and the rare instances of bad steric overlap in these high-accuracy structures. Kinemage 3D display files were made with the "multi-criterion" function in MolProbity, which highlights alternate conformations, poor rotamers (Lovell et al., 2000), Ramachandran outliers (Lovell et al., 2003), and serious all-atom clashes (overlaps $\geq$0.4 Å), with user-controllable extra detail. The multi-criterion kinemages were viewed in the KiNG Java display program (Davis et al., 2004), along with $2F_o - F_c$ and $F_o - F_c$ maps obtained from the Electron Density Server at http://eds.bmc.uu.se (Kleywegt et al., 2004).

For each protein, Table 1 lists the number of residues for which an alternate conformation was defined for at least one atom (569/3882 residues total, or 15%). Alternate conformations involving concerted movement for the backbone of two or more neighboring residues were not analyzed in this study; omitting those 24 cases (93 residues) gives the 476 single-residue alternates. All single residues with alternate conformations defined for the Cβ atom (404 residues) are potential candidates for backbone movement, because a true shift of Cβ means the backbone must have moved, although small backbone changes are often modeled only as anisotropic B factors. After a preliminary survey, it was determined that a shift of at least 0.2 Å in Cβ position was necessary in order to draw unambiguous conclusions about the specific changes in backbone conformation. A total of 200 single-residue alternates had Cβ shifts $\geq$0.2 Å (see Table 1). A total of 34 of them were omitted; half were not relevant because both sidechain conformations could actually be well fit from a single ideal Cβ position, implying no backbone motion (e.g., 1N9B Leu30, shown in the Additional Data; 1SSX Met213), while, for the others, electron density for the lower-occupancy conformation was visible for too few atoms or was too poorly shaped to allow reliable inferences about the geometry of backbone changes (e.g., 1GWE Val217, 1EJG Pro36, 1US0 Glu64 and Lys307). The 166 clearly interpretable single-residue examples with verified Cβ shifts $\geq$ 0.2Å were then classified as exhibiting either backrub movement (as described below) or some other type of movement.

Definition of Backrub Movement and Backrub Modeling

A backrub motion shifts the position of the Cα-Cβ bond vector for residue *i* by a backbone change that is low energy (i.e., maintains essentially ideal bond lengths, bond angles, and peptide planarity) and is purely local (i.e., with essentially no motion of C$\alpha_{i\pm1}$ and none at all

beyond $C\alpha_{i\pm2}$). The Backrub modeling algorithm, described below, closely satisfies the backrub paradigm by using three rotations around $C\alpha$-$C\alpha$ axes. Successful modeling of a putative backrub motion with the Backrub software means that all clearly visible sidechain and backbone atom positions in both conformations can be well fit by two states of a single, closely ideal model that differ only by adjustment of the three variable Backrub parameters, plus χ angles for sidechain *i*.

BACKRUB Algorithm for Software Tools

A preliminary exploration of backrub motions was done by a brute-force sampling of ϕ,ψ,τ space that built model halves separately inward from $C\alpha_{i-1}$ and $C\alpha_{i+1}$ to meet at a resulting $C\alpha_i$ within 0.02 Å, disallowing Ramachandran outliers and limiting nonideality of τ (Figure 4). This search produces a fan of permissible conformations that swing the central $C\alpha$-$C\beta$ vector perpendicular to the chain direction, as anticipated, with essentially no $C\beta$ motion in other directions. However, the ϕ,ψ plots of Figure 4 show that the relationships are nonlinear and complex. The curve shapes differ for different starting conformations and for residue *i*−1 versus *i*+1, and they show much more spread with variation of $\tau_{i\pm1}$ in the β than in the α region. (Banding is an artifact of a 3° sampling interval in τ.) Interestingly, ϕ and ψ change very little for the central residue *i* whose sidechain is moving. These complex relationships prevented derivation of an analytical expression for this motion.

The simplified Backrub algorithm (Figure 1) was developed for practical use, with only three independent variables. It produces an extremely close approximation of a backrub motion by user control of rigid-body rotations around $C\alpha$-$C\alpha$ vectors: a two-peptide rotation and two single-peptide rotations. The Backrub algorithm was implemented in Java as a tool in KiNG. Its use requires specifying the appropriate PDB-format coordinate file (with hydrogens) and activates a dialog box to control the rotations, with informational displays that warn of Ramachandran outliers (Lovell et al., 2003) or τ angles > 1σ from ideal (Engh and Huber, 1991). The Backrub tool can be active at the same time as the sidechain rotamer and rotation tool in KiNG, which is similar to the sidechain tool described for Mage (Richardson et al., 2003; Word et al., 2000). The KiNG software and related programs are available, free, and open-source from http://kinemage.biochem.duke.edu.

The geometry used by the Backrub algorithm is diagrammed in Figure 1A. It acts on a central residue *i* and the two flanking peptides. For each of three different rotational components, a subgroup of atoms moves as a rigid body around some (virtual) axis. The primary component of motion rotates all atoms between the $C\alpha$s of residue *i*−1 and *i*+1 around an axis between $C\alpha_{i-1}$ and $C\alpha_{i+1}$. This produces a wide arcing motion of the sidechain roughly perpendicular to the overall local chain direction. The two secondary components rotate the four central atoms of a peptide group around an axis between the $C\alpha$s on either end, which helps alleviate τ angle or H bond strain introduced by the primary motion. All bond lengths and angles are invariant, except for the three τ angles. In Figure 1B, the substates differ only by the primary rotation, while in Figure 1C the peptides have been rotated to help preserve the H bonding CO and NH positions.

The Backrub algorithm closely approximates the common backrub mode of local backbone plasticity (see Discussion). However, it should be noted that there are many other changes in backbone conformation to which it is not applicable. Its area of effect is deliberately small, and so it is not suited for motions of large chain segments. Since it assumes fixed anchor points at either end, it cannot be used for domain hinges or immediately next to chain ends. A generalization of Backrub to act between arbitrary $C\alpha$s was explored, but it introduces further complications while adding only a few additional successes at fitting changes in longer loops.

To aid in the assignment of backrub motion versus other motion for each alternate conformation example, modeling of changes was tested by using the Backrub tool in KiNG for more than half of the 166 cases, including all large or complex motions and multiple examples of each recognizable pattern of change (e.g., serines similar to Figure 2B). If backbone atoms had been assigned alternate positions in the PDB file, then the conformation with more ideal peptide geometry (usually A) was taken as the starting point for modeling the second (B) alternate conformation, using only the three Backrub rotations and the sidechain χ dihedrals with idealized sidechain geometry, and emphasizing fit to the atoms most clearly observed in the electron density. In some cases, both original conformations had substantial, but opposite, distortions in covalent geometry; a more nearly ideal intermediate would make a better Backrub starting point, but we very seldom added such a step (e.g., Kin. 6 in the Additional Data). The criteria of good fit were the same as would be applied in crystallographic rebuilding at this resolution. If alternates had been assigned starting only at $C\beta$, then the common backbone conformation was taken as the starting point, with an idealized $C\beta$ (Lovell et al., 2003) (usually halfway between the two assigned $C\beta$ positions) and ideal-geometry sidechain (Engh and Huber, 1991); then both A and B conformations were modeled with Backrub motions in opposite directions. These Backrub models are shown in orange in the figures, where their fit to deposited models and to electron density can be judged.

For correction of an experimental model misfit into the wrong local minimum conformation during crystallographic refinement (e.g., Figure 3), first the new sidechain rotamer was chosen, next the backbone was shifted with the Backrub tool, and finally both backbone and sidechain rotations were adjusted to optimize all-atom contacts and electron density fit.

Additional Data

Additional Data include a Readme file explaining the kinemage and PDB files, animated 3D kinemages of six backrub examples, and the PDB-format coordinates for ten examples. These files are available at http://kinemage.biochem.duke.edu/suppinfo/StructureDavis2006.

Supplemental Data

Supplemental Data, including a table of the 126 backrubs and a list of Additional Data available from the authors, are available at http://www.structure.org/cgi/content/full/14/2/265/DC1/.

Acknowlegements

We thank Wolfram Tempel and B.C. Wang for SECSG collaboration on using the Backrub tool in structure improvement, Jack Snoeyink for collaboration on inverse kinematics of protein backbone, Gerard Kleywegt for providing $F_o - F_c$ as well as $2F_o - F_c$ maps on the Electron Density Server site, and the crystallographers who deposited these high-resolution structures and data. Support was from National Institutes of Health GM-073930, GM-15000, P50 GM-62407, and a HHMI Predoctoral Fellowship to I.W.D.

Received: August 6, 2005
Revised: October 10, 2005
Accepted: October 12, 2005
Published: February 10, 2006

References

Addlagatta, A., Krzywda, S., Czapinska, H., Otlewski, J., and Jaskolski, M. (2001). Ultrahigh-resolution structure of a BPTI mutant. Acta Crystallogr. D Biol. Crystallogr. *57*, 649–663.

Arendall, W.B., III, Tempel, W., Richardson, J.S., Zhou, W., Wang, S., Davis, I.W., Liu, Z.J., Rose, J.P., Carson, M., Luo, M., et al. (2005). A test of enhancing model accuracy in high-throughput crystallography. J. Struct. Funct. Genomics *6*, 1–11.

Bahar, I., Erman, B., Haliloglu, T., and Jernigan, R.L. (1997). Efficient characterization of collective motions and interresidue correlations in proteins by low-resolution simulations. Biochemistry *36*, 13512–13523.

Baldwin, E.P., Hajiseyedjavadi, O., Baase, W.A., and Matthews, B.W. (1993). The role of backbone flexibility in the accommodation of variants that repack the core of T4 lysozyme. Science *262*, 1715–1718.

Berman, H.M., Westbrook, J., Feng, Z., Gilliland, G., Bhat, T.N., Weissig, H., Shindyalov, I.N., and Bourne, P.E. (2000). The Protein Data Bank. Nucleic Acids Res. *28*, 235–242.

Blaszczyk, J., Li, Y., Shi, G., Yan, H., and Ji, X. (2003). Dynamic roles of arginine residues 82 and 92 of *Escherichia coli* 6-hydroxymethyl-7,8-dihydropterin pyrophosphokinase: crystallographic studies. Biochemistry *42*, 1573–1580.

Cavanagh, J., Fairbrother, W.J., Palmer, A.G., III, and Skelton, N.J. (1996). Protein NMR Spectroscopy: Principles and Practice (San Diego: Academic Press).

Chou, J.J., Case, D.A., and Bax, A. (2003). Insights into the mobility of methyl-bearing side chains in proteins from (3)J(CC) and (3)J(CN) couplings. J. Am. Chem. Soc. *125*, 8959–8966.

Dahiyat, B.I., and Mayo, S.L. (1997). *De novo* protein design: fully automated sequence selection. Science *278*, 82–87.

Davis, I.W., Murray, L.W., Richardson, J.S., and Richardson, D.C. (2004). MOLPROBITY: structure validation and all-atom contact analysis for nucleic acids and their complexes. Nucleic Acids Res. *32*, W615–W619.

DePristo, M.A., de Bakker, P.I.W., Lovell, S.C., and Blundell, T.L. (2003). Ab initio construction of polypeptide fragments: efficient generation of accurate, representative ensembles. Proteins *51*, 41–55.

Desjarlais, J.R., and Handel, T.M. (1995). *De novo* design of the hydrophobic cores of proteins. Protein Sci. *4*, 2006–2018.

Engh, R.A., and Huber, R. (1991). Accurate bond and angle parameters for X-ray protein structure refinement. Acta Crystallogr. A *47*, 392–400.

Engh, R.A., and Huber, R. (2002). Structure quality and target parameters. In International Tables for Crystallography, Volume F, M.G. Rossman, and E. Arnold, eds. (Dordrecht: Kluwer Academic Publishers), pp. 382–392.

Erskine, P.T., Coates, L., Mall, S., Gill, R.S., Wood, S.P., Myles, D.A., and Cooper, J.B. (2003). Atomic resolution analysis of the catalytic site of an aspartic proteinase and an unexpected mode of binding by short peptides. Protein Sci. *12*, 1741–1749.

Esposito, L., Vitagliano, L., Sica, F., Sorrentino, G., Zagari, A., and Mazzarella, L. (2000). The ultrahigh resolution crystal structure of ribonuclease A containing an isoaspartyl residue: hydration and sterochemical analysis. J. Mol. Biol. *297*, 713–732.

Fadel, A.R., Jin, D.Q., Montelione, G.T., and Levy, R.M. (1995). Crankshaft motions of the polypeptide backbone in molecular dynamics simulations of human type-α transforming growth factor. J. Biomol. NMR *6*, 221–226.

Fenn, T.D., Ringe, D., and Petsko, G.A. (2004). Xylose isomerase in substrate and inhibitor michaelis states: atomic resolution studies of a metal-mediated hydride shift. Biochemistry *43*, 6464–6474.

Fuhrmann, C.N., Kelch, B.A., Ota, N., and Agard, D.A. (2004). The 0.83 Å resolution crystal structure of alpha-lytic protease reveals the detailed structure of the active site and identifies a source of conformational strain. J. Mol. Biol. *338*, 999–1013.

Gassner, N.C., Baase, W.A., and Matthews, B.W. (1996). A test of the "jigsaw puzzle" model for protein folding by multiple methionine substitutions within the core of T4 lysozyme. Proc. Natl. Acad. Sci. USA *93*, 12155–12158.

Getzoff, E.D., Gutwin, K.N., and Genick, U.K. (2003). Anticipatory active-site motions and chromophore distortion prime photoreceptor PYP for light activation. Nat. Struct. Biol. *10*, 663–668.

Howard, E.I., Sanishvili, R., Cachau, R.E., Mitschler, A., Chevrier, B., Barth, P., Lamour, V., Van Zandt, M., Sibley, E., Bon, C., et al. (2004). Ultrahigh resolution drug design I: details of interactions in human aldose reductase-inhibitor complex at 0.66 Å. Proteins *55*, 792–804.

Hu, H., Elstner, M., and Hermans, J. (2003). Comparison of a QM/MM force field and molecular mechanics force fields in simulations of alanine and glycine 'dipeptides' (Ace-Ala-Nme and Ace-Gly-Nme) in water in relation to the problem of modeling the unfolded peptide backbone in solution. Proteins *50*, 451–463.

Jelsch, C., Teeter, M.M., Lamzin, V., Pichon-Lesme, V., Blessing, R.H., and Lecomte, C. (2000). Accurate protein crystallography at ultra-high resolution: valence-electron distribution in crambin. Proc. Natl. Acad. Sci. USA *97*, 3171–3176.

Kang, B.S., Devedjiev, Y., Derewenda, U., and Derewenda, Z.S. (2004). The PDZ2 domain of syntenin at ultra-high resolution: bridging the gap between macromolecular and small molecule crystallography. J. Mol. Biol. *338*, 483–493.

Karplus, M., and McCammon, J.A. (2002). Molecular dynamics simulations of biomolecules. Nat. Struct. Biol. *9*, 646–652.

Kay, L.E. (2005). NMR studies of protein structure and dynamics. J. Magn. Reson. *173*, 193–207.

Kleywegt, G.J. (1999). Experimental assessment of differences between related protein crystal structures. Acta Crystallogr. D Biol. Crystallogr. *55*, 1878–1884.

Kleywegt, G.J., Harris, M.R., Zou, J.Y., Taylor, T.C., Wahlby, A., and Jones, T.A. (2004). The Uppsala electron-density server. Acta Crystallogr. D Biol. Crystallogr. *60*, 2240–2249.

Ko, T.P., Robinson, H., Gao, Y.G., Cheng, C.H., DeVries, A.L., and Wang, A.H. (2003). The refined crystal structure of an eel pout type III antifreeze protein RD1 at 0.62-Å resolution reveals structural microheterogeneity of protein and solvation. Biophys. J. *84*, 1228–1237.

Kursula, I., and Wierenga, R.K. (2003). Crystal structure of triosephosphate isomerase complexed with 2-phosphoglycolate at 0.83-Å resolution. J. Biol. Chem. *278*, 9544–9551.

Lim, W.A., and Sauer, R.T. (1989). Alternative packing arrangements in the hydrophobic core of λ repressor. Nature *339*, 31–36.

Lipari, G., Szabo, A., and Levy, R.M. (1982). Protein dynamics and NMR relaxation: comparison of simulations with experiment. Nature *300*, 197–198.

Liu, L., Nogi, T., Kobayashi, M., Nozawa, T., and Miki, K. (2002). Ultrahigh-resolution structure of high-potential iron-sulfur protein from *Thermochromatium tepidum*. Acta Crystallogr. D Biol. Crystallogr. *58*, 1085–1091.

Liu, Q., Huang, Q., Teng, M., Weeks, C.M., Jelsch, C., Zhang, R., and Niu, L. (2003). The crystal structure of a novel, inactive, lysine 49 PLA2 from *Agkistrodon acutus* venom: an ultrahigh resolution, ab initio structure determination. J. Biol. Chem. *278*, 41400–41408.

Looger, L.L., Dwyer, M.A., Smith, J.J., and Hellinga, H.W. (2003). Computational design of receptor and sensor proteins with novel functions. Nature *423*, 185–190.

Lovell, S.C., Word, J.M., Richardson, J.S., and Richardson, D.C. (2000). The penultimate rotamer library. Proteins *40*, 389–408.

Lovell, S.C., Davis, I.W., Arendall, W.B., III, de Bakker, P.I.W., Word, J.M., Prisant, M.G., Richardson, J.S., and Richardson, D.C. (2003). Structure validation by Cα geometry: ϕ,ψ and Cβ deviation. Proteins *50*, 437–450.

Matthews, B.W. (1995). Studies on protein stability with T4 lysozyme. Adv. Protein Chem. *46*, 249–278.

Mooers, B.H., Datta, D., Baase, W.A., Zollars, E.S., Mayo, S.L., and Matthews, B.W. (2003). Repacking the core of T4 lysozyme by automated design. J. Mol. Biol. *332*, 741–756.

Munson, M., O'Brien, R., Sturtevant, J.M., and Regan, L. (1994). Redesigning the hydrophobic core of a four-helix-bundle protein. Protein Sci. *3*, 2015–2022.

Murshudov, G.N., Grebenko, A.I., Brannigan, J.A., Antson, A.A., Barynin, V.V., Dodson, G.G., Dauter, Z., Wilson, K.S., and Melik-Adamyan, W.R. (2002). The structures of *Micrococcus lysodeikticus* catalase, its ferryl intermediate (compound II) and NADPH complex. Acta Crystallogr. D Biol. Crystallogr. *58*, 1972–1982.

Noonan, K., O'Brien, D., and Snoeyink, J. (2004). Probik: Protein Backbone Motion by Inverse Kinematics. Paper presented at: Workshop on the Algorithmic Foundations of Robotics (Springer Verlag).

Nukaga, M., Mayama, K., Hujer, A.M., Bonomo, R.A., and Knox, J.R. (2003). Ultrahigh resolution structure of a class A β-lactamase: on the mechanism and specificity of the extended-spectrum SHV-2 enzyme. J. Mol. Biol. *328*, 289–301.

Palmer, A.G., III (2004). NMR characterization of the dynamics of biomacromolecules. Chem. Rev. *104*, 3623–3640.

Palmo, K., Mannfors, B., Mirkin, N.G., and Krimm, S. (2003). Potential energy functions: from consistent force fields to spectroscopically determined polarizable force fields. Biopolymers *68*, 383–394.

Patterson, W.R., Anderson, D.H., DeGrado, W.F., Cascio, D., and Eisenberg, D. (1999). Centrosymmetric bilayers in the 0.75 Å resolution structure of a designed α-helical peptide, D,L-Alpha-1. Protein Sci. *8*, 1410–1422.

Qian, B., Ortiz, A.R., and Baker, D. (2004). Improvement of comparative model accuracy by free-energy optimization along principal

components of natural structural variation. Proc. Natl. Acad. Sci. USA *101*, 15346–15351.

Richardson, J.S., and Richardson, D.C. (1988). Amino acid preferences for specific locations at the ends of α-helices. Science *240*, 1648–1652.

Richardson, J.S., Richardson, D.C., Tweedy, N.B., Gernert, K.M., Quinn, T.P., Hecht, M.H., Erickson, B.W., Yan, Y., McClain, R.D., Donlan, M.E., and Surles, M.C. (1992). Looking at proteins: representations, folding, packing, and design. Biophys. J. *63*, 1186–1209.

Richardson, J.S., Arendall, W.B., III, and Richardson, D.C. (2003). New tools and data for improving structures, using all-atom contacts. In Methods in Enzymology, Volume 374, C.W. Carter, Jr., and R.M. Sweet, eds. (New York: Academic Press), pp. 385–412.

Rohl, C.A., Strauss, C.E., Misura, K.M., and Baker, D. (2004). Protein structure prediction using Rosetta. Methods Enzymol. *383*, 66–93.

Schmidt, A., Jelsch, C., Ostergaard, P., Rypniewski, W., and Lamzin, V.S. (2003). Trypsin revisited: crystallography at (sub) atomic resolution and quantum chemistry revealing details of catalysis. J. Biol. Chem. *278*, 43357–43362.

Schneider, T.R., and Sheldrick, G.M. (2002). Substructure solution with SHELXD. Acta Crystallogr. D Biol. Crystallogr. *58*, 1772–1779.

Tramontano, A., and Morea, V. (2003). Assessment of homology-based predictions in CASP5. Proteins *53* (*Suppl 6*), 352–368.

van den Bedem, H., Lotan, I., Latombe, J.C., and Deacon, A.M. (2005). Real-space protein-model completion: an inverse-kinematics approach. Acta Crystallogr. D Biol. Crystallogr. *61*, 2–13.

Wang, T., Cai, S., and Zuiderweg, E.R. (2003). Temperature dependence of anisotropic protein backbone dynamics. J. Am. Chem. Soc. *125*, 8639–8643.

Word, J.M., Lovell, S.C., LaBean, T.H., Taylor, H.C., Zalis, M.E., Presley, B.K., Richardson, J.S., and Richardson, D.C. (1999a). Visualizing and quantifying molecular goodness-of-fit: small-probe contact dots with explicit hydrogens. J. Mol. Biol. *285*, 1711–1733.

Word, J.M., Lovell, S.C., Richardson, J.S., and Richardson, D.C. (1999b). Asparagine and glutamine: using hydrogen atom contacts in the choice of side-chain amide orientation. J. Mol. Biol. *285*, 1735–1747.

Word, J.M., Bateman, R.C., Jr., Presley, B.K., Lovell, S.C., and Richardson, D.C. (2000). Exploring steric constraints on protein mutations using Mage/Probe. Protein Sci. *9*, 2251–2259.

Wuthrich, K. (1986). NMR of Proteins and Nucleic Acids (New York: Wiley).